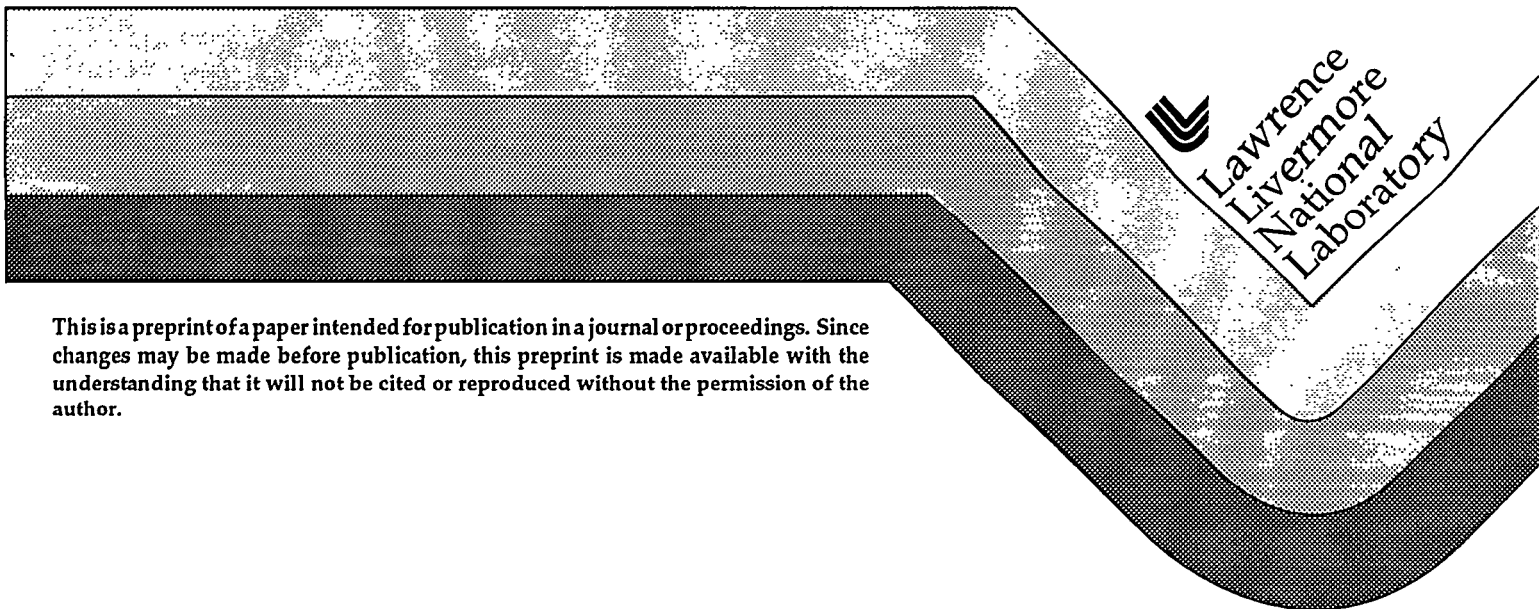


# Experiments and Modeling with a Large-Area Inductively Coupled Plasma (ICP) Source

R.D. Benjamin  
G. DiPeso  
P.O. Egan  
G.J. Parker  
R.A. Richardson  
P. Vitello

This paper was prepared for submittal to the  
*Third International Workshop on Advanced Plasma Tools*  
*San Jose, CA*  
*May 3-4, 1995*

June 1995



This is a preprint of a paper intended for publication in a journal or proceedings. Since changes may be made before publication, this preprint is made available with the understanding that it will not be cited or reproduced without the permission of the author.

#### DISCLAIMER

This document was prepared as an account of work sponsored by an agency of the United States Government. Neither the United States Government nor the University of California nor any of their employees, makes any warranty, express or implied, or assumes any legal liability or responsibility for the accuracy, completeness, or usefulness of any information, apparatus, product, or process disclosed, or represents that its use would not infringe privately owned rights. Reference herein to any specific commercial products, process, or service by trade name, trademark, manufacturer, or otherwise, does not necessarily constitute or imply its endorsement, recommendation, or favoring by the United States Government or the University of California. The views and opinions of authors expressed herein do not necessarily state or reflect those of the United States Government or the University of California, and shall not be used for advertising or product endorsement purposes.

## **DISCLAIMER**

**Portions of this document may be illegible in electronic image products. Images are produced from the best available original document.**

# Experiments and Modeling with a Large-Area Inductively Coupled Plasma (ICP) Source

R.D. Benjamin, G. DiPeso, P.O. Egan,  
G.J. Parker, R.A. Richardson and P. Vitello



Lawrence Livermore National Laboratory

3rd International Workshop on Advanced Plasma Tools  
San Jose, May 3-4, 1995

## Abstract

We describe initial experiments with a large (30") plasma source chamber to explore the problems associated with large-area inductively coupled plasma (ICP) sources to produce high density plasmas useful for processing 400 mm semiconductor wafers. Our experiments typically use a 25" diameter planar ICP coil driven at 13.56 MHz. Plasma and system data are taken in Ar and N<sub>2</sub> over the pressure range 3-50 mtorr. R.F. inductive power was run up to 2000W, but typically data were taken over the range 100-1000W. Diagnostics include optical emission spectroscopy, Langmuir probes, and B-dot probes as well as electrical circuit measurements. The B-dot and E-M measurements are compared with models based on commercial E-M codes. Initial indications are that uniform plasmas suitable for 400 mm processing are attainable.

We present a comparison between computer modeling and experimental results for this source. Computer simulations using the fluid code INDUCT94 are used to explain variations in the plasma density profile measurements as a function of inductive power, gas pressure and gas composition. Both Argon and Nitrogen discharges are modeled. INDUCT94 solves the 2D time-dependent fluid equations for electrons, ions and neutrals including effects of both inductive and capacitive coupling. Detailed volume and surface chemistry reactions are treated. We discuss the effects of pressure and power on plasma uniformity.

### Acknowledgments

Work performed under the auspices of Department of Energy at Lawrence Livermore National Laboratory under contract W-7405-ENG-48.

## Overview

### Goals

- Develop uniform large-area ICP plasma source for potential 12" to 16" wafer and FPD applications.
- Initial plasma development experiments with Ar and N<sub>2</sub>
- Coordinate experiments and modeling effort for synergy.
- ICP development on test chamber. We are now constructing a process chamber for Cl<sub>2</sub> etch experiments.

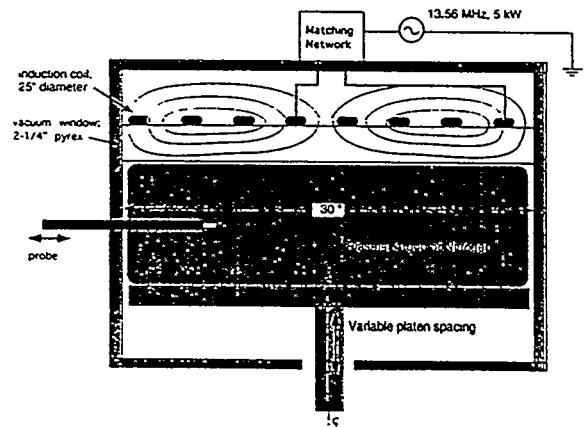
### Features

- 30" diameter chamber
- 25" diameter ICP coil
- 2 or 2-1/4" thick dielectric window
- Rf drive: 13.56 MHz to 5kW
- Ar or N<sub>2</sub> at 3 to 50 mtorr

### Diagnostics

- Langmuir probes
- B-dot probes
- Electrical measurements
- Optical spectroscopy

## Inductively Coupled Plasma Etch Tool



MASTER

DISTRIBUTION OF THIS DOCUMENT IS UNLIMITED

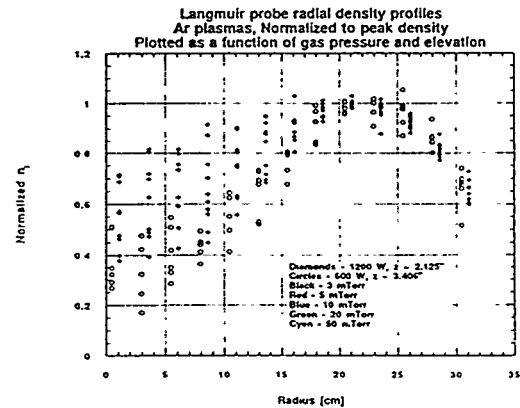
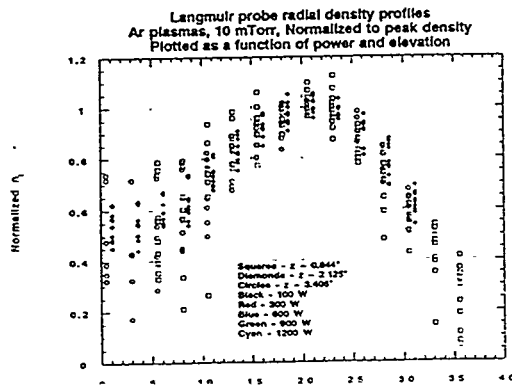
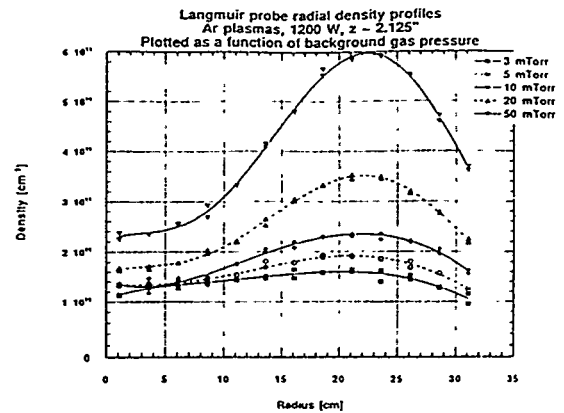
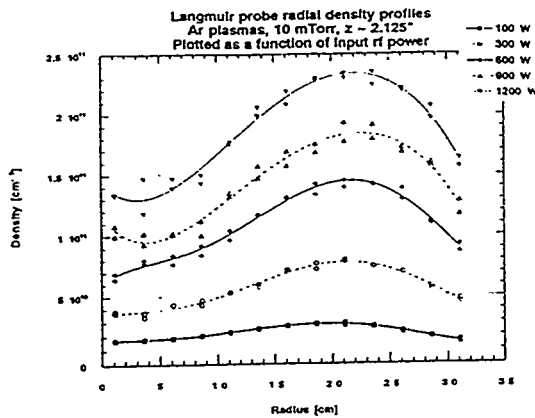
## Density profiles in Ar plasmas

These figures show the ion density profiles in Ar plasmas determined from Langmuir probe measurements. The density profiles are plotted as a function of both input rf power and background gas pressure. Normalized ion density profiles are shown at different elevations within the plasma chamber as functions of these same parameters.

Electron densities are also determined from the Langmuir probe I-V curve. The radial electron density profiles exhibit a shape similar to that of the ion profiles, but the magnitudes do not always agree. These differences are presently being investigated.

The plasma density increases as the input rf power is raised, but the shape of the profile is unaffected by the rf power level (except perhaps at the lowest rf powers). The density profiles are not peaked on axis, due to the presence of localized heating under the rf coils and the mean free path in Ar at 10 mTorr, which is short enough to limit the ability of diffusion to flatten the profiles.

The plasma density also increases as the background gas pressure is raised. In addition, raising the background gas pressure increases the off axis density faster than the central density, thereby making the density profile more hollow. This is a direct result of the decrease in the mean free path as the gas pressure is raised, which slows down diffusion.



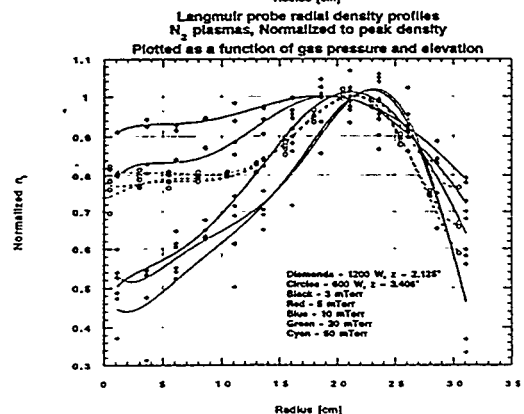
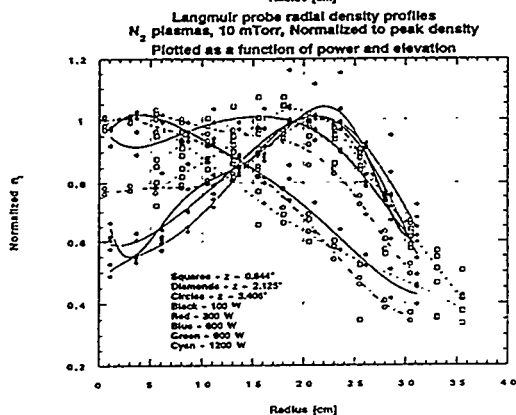
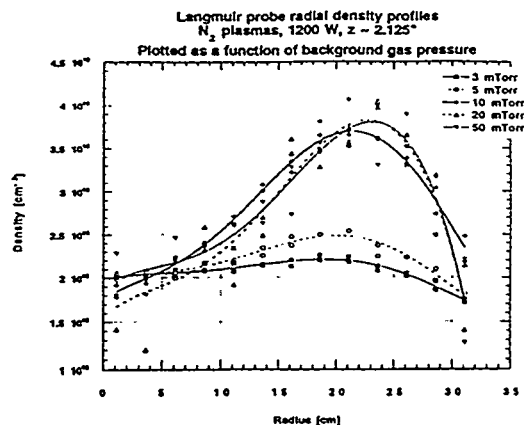
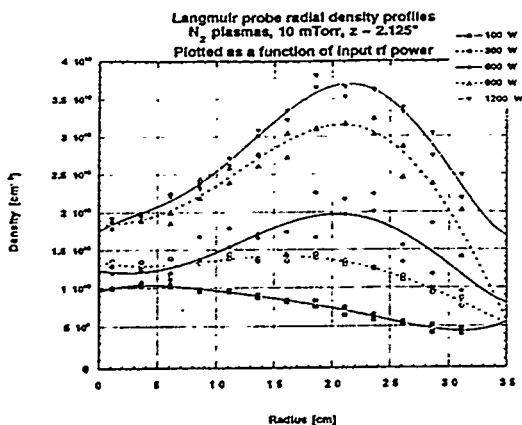
## Density profiles in N<sub>2</sub> plasmas

These figures show the ion density profiles in N<sub>2</sub> plasmas determined from Langmuir probe measurements. The density profiles are plotted as a function of both input rf power and background gas pressure. Normalized ion density profiles are shown at different elevations within the plasma chamber as functions of these same parameters.

Electron densities are also determined from the Langmuir probe I-V curve. The radial electron density profiles exhibit a shape similar to that of the ion profiles, but the magnitudes do not always agree. These differences are presently being investigated.

As in Ar plasmas, the plasma density increases as the input rf power is raised. In contrast to the Ar results, the shape of the profile in N<sub>2</sub> plasmas is strongly affected by the rf power level. The density profiles are peaked on axis at the lowest rf powers and become peaked off axis at higher powers. The reason for this change in the shape of the density profile is believed to be due to the low value of the density in these plasmas, leading to a large skin depth and non-localized heating. The same effect should be seen in Ar plasmas, but experimentally we cannot operate the machine under these conditions.

The plasma density also increases as the background gas pressure is raised. In addition, raising the background gas pressure increases the off axis density faster than the central density, thereby making the density profile more hollow. This is a direct result of the decrease in both the mean free path as the gas pressure is raised, which limits the ability of diffusion to flatten the profiles, and the skin depth of the plasma, which gives rise to localized heating.



## Electric Field and Plasma Conductivity from B-dot Data

Start with Faraday's equation.  $\nabla \times \mathbf{E} = -\dot{\mathbf{B}} = -j\omega \mathbf{B}$

assume  $\mathbf{B} = B_z(r,z)\mathbf{z} + B_r(r,z)\mathbf{r} = (B_z(r)z + B_r(r)r) \exp(-z/\delta)$

$\mathbf{E} = E_\theta(r,z)\boldsymbol{\theta}$

Then Faraday's equation becomes:

$$-dE_\theta/dz = -j\omega B_r = 1/\delta E_\theta, \text{ where } \delta \text{ is skin depth} = (\sigma\omega\mu_0/2)^{-1/2}$$

$$-1/r d/dr(rE_\theta) = -j\omega B_z$$

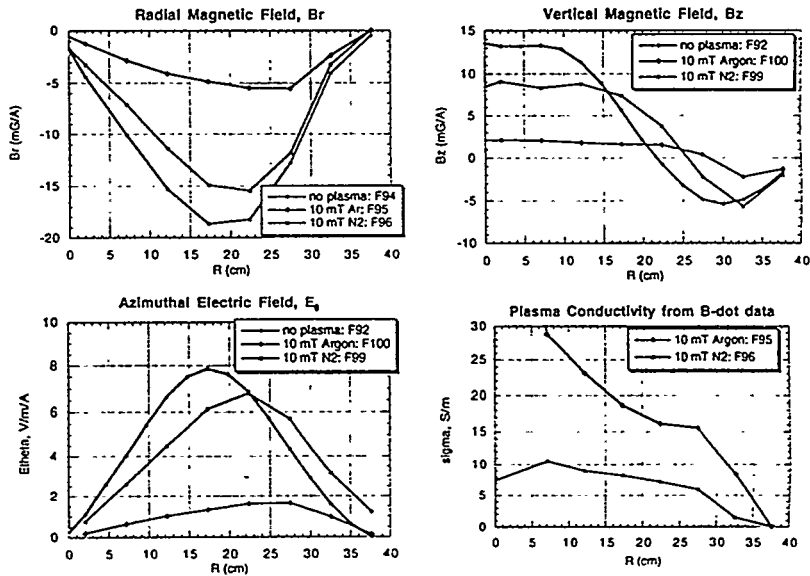
Then I get the electric field in the plasma by integrating the z component of the magnetic field.

$$E_\theta = -j\omega r \int_0^r B_z r' dr'$$

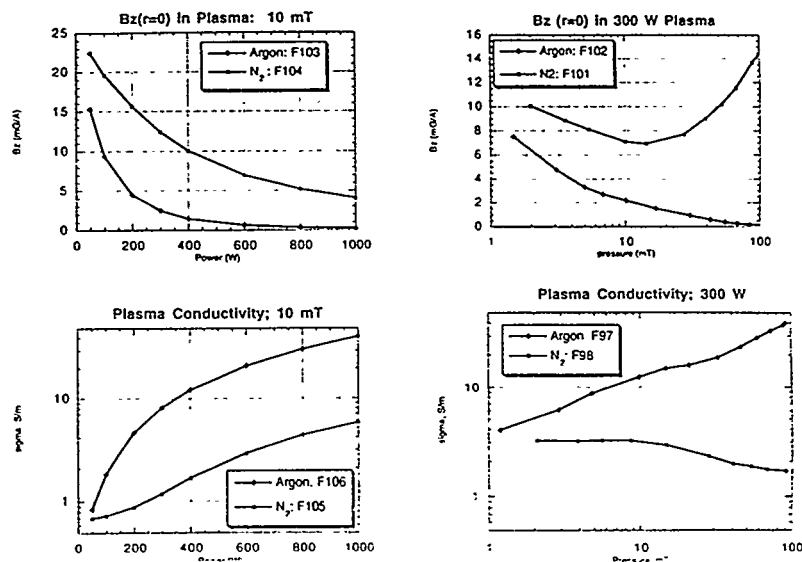
The conductivity of the plasma can be had by dividing the electric field by the Br component

$$\sigma = (B_r/E_\theta)^2 2\omega\mu_0$$

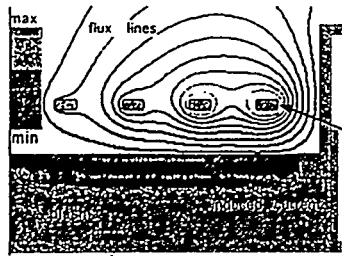
### Bdot Data: Bz, Br, Etheta, Conductivity



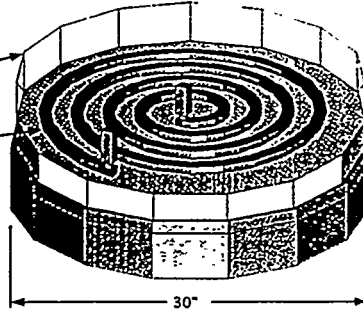
### Bdot Data: Power and Pressure vs Bz



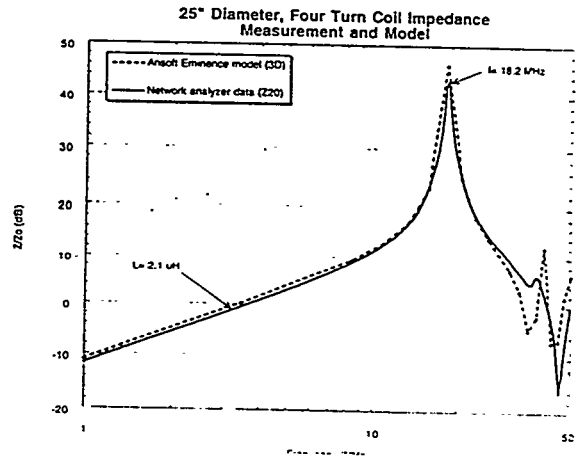
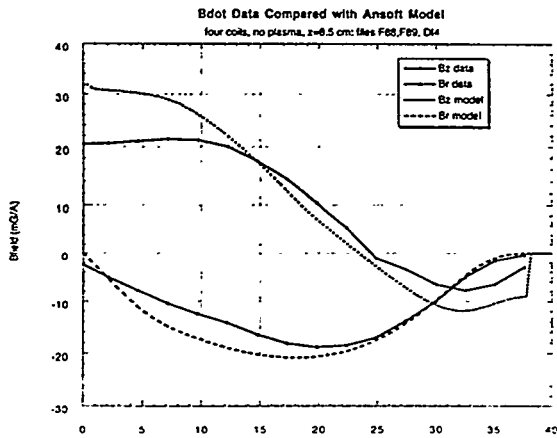
# Electromagnetic Code Modeling



2D Model (Ansoft Maxwell)  
 Quasi-magnetostatic (eddy current) solver  
 Solved flux lines and induced current shown  
 RF frequency,  $f_0 = 13.56$  MHz  
 Plasma conductivity = 30 mho/m

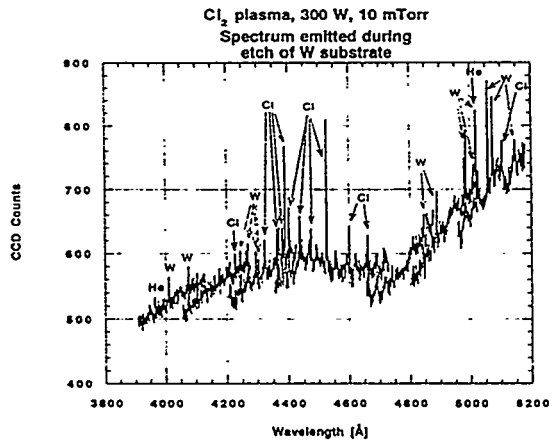
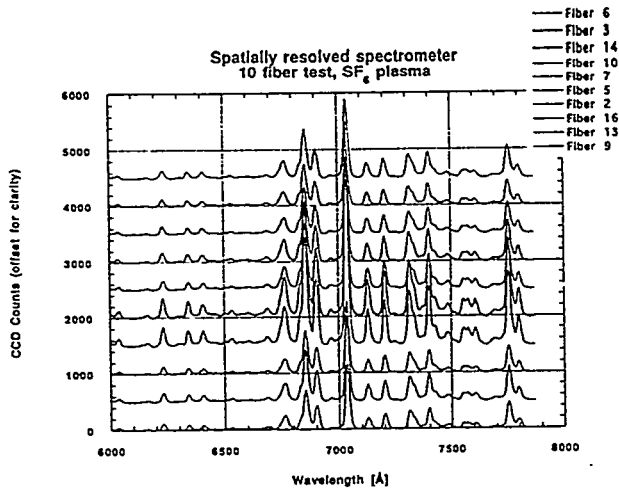
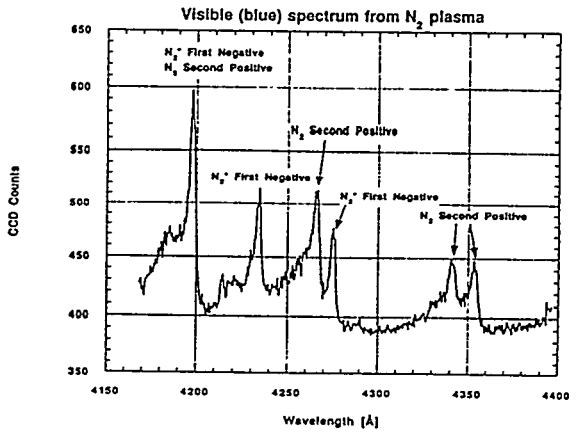


3D Model (Ansoft Eminence)  
 Full wave solver  
 Simplified geometry



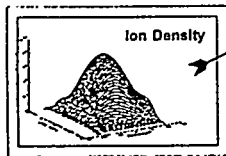
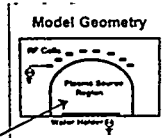
### Spectroscopy Goals

- Spectroscopy is a truly non-invasive diagnostic. It requires only a small viewport for viewing the plasma chamber.
- We hope to find temperature and density sensitive line ratios. This would provide independent verification of Langmuir probe measurements. In addition, it would allow measurements to be made in systems where probe measurements are not practical (e.g., process reactors).
- Spatially resolved measurements should provide a determination of plasma uniformity. Unfortunately, most of the lines observed thus far have been emitted by the neutral background gas rather than a plasma constituent (except for emissions from  $N_2^+$ ). We need to verify that these neutral emissions exhibit the same spatial dependence as the plasma density.
- Real time analysis of the plasma emission spectrum may prove useful in process control.



## INDUCT94- Inductively Coupled Plasma Source Model

- 2D time-dependent fluid model.
- Electrons, multiple ions and neutrals.
- Single frequency RF coils.
- RF bias on wafer holder.
- Complex internal structures.



- Ion and electron temperatures.
- Neutral flow.
- Electronegative and electro-positive plasmas.
- Optimized for high efficiency.

## Ion Model Equations

- Density,  $n_i$ , solved from continuity equation:

$$\partial n_i / \partial t = -\nabla \cdot \bar{\Gamma}_i + R_{\text{ionization}}$$

- Flux,  $\bar{\Gamma}_i = n_i \bar{v}_i$ , solved from momentum equation:

$$\partial \bar{\Gamma}_i / \partial t = -\nabla \cdot \bar{\Gamma}_i \bar{v}_i + en_i \bar{E} / m_i - (\bar{v} n_i k T_i) / m_i - n_i v_{\text{in}} \bar{v}_i$$

- Temperature,  $T_i$ , solved from energy equation:

$$\partial T_i / \partial t = -\nabla \cdot \bar{Q}_i - en_i \bar{\Gamma}_i \cdot \bar{E}$$

## Electron Model Equations

- Density,  $n_e$ , solved from continuity equation:

$$\partial n_e / \partial t = -\nabla \cdot \bar{\Gamma}_e + R_{\text{ionization}}$$

- Flux,  $\bar{\Gamma}_e = n_e \bar{v}_e$ , calculated from "drift-diffusion" approximation:

$$\bar{\Gamma}_e = -n_e \mu_e \bar{E} - (\bar{v} n_e k T_e) / m_e v_{eN}$$

- Temperature,  $T_e$ , solved from energy equation:

$$\partial T_e / \partial t = -\nabla \cdot \bar{Q}_e - en_e \bar{\Gamma}_e \cdot \bar{E} + P_{\text{in}} - \Lambda_{\text{loss}}$$

## Poisson's Equation

- The potential,  $\phi$ , is solved from from a time-advanced form of Poisson's equation:

$$\nabla \cdot \epsilon \nabla \phi = -e(n_i - n_e - \delta t \partial n_e / \partial t)$$

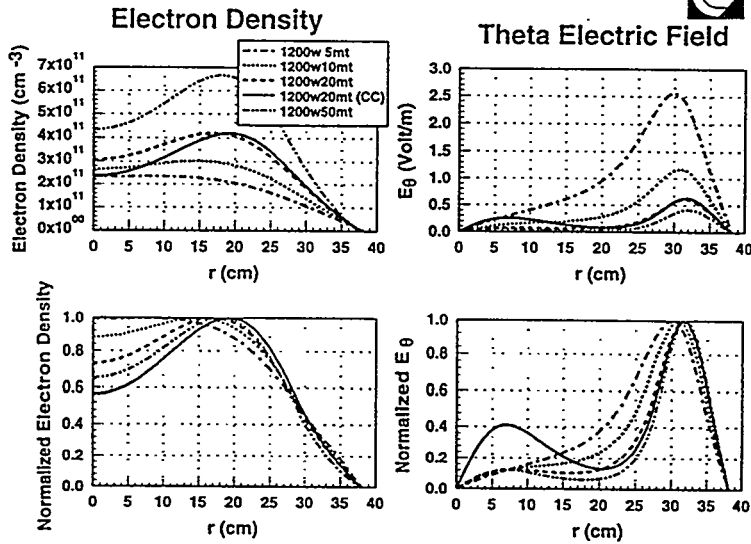
- Use of the electron continuity equation:

- ✦ Enforces strong implicit coupling between the electric field and the electron density.
- ✦ Avoids the Dielectric relaxation time-scale instability.
- ✦ Provides for quasi-neutrality, and near ambi-polar flow.

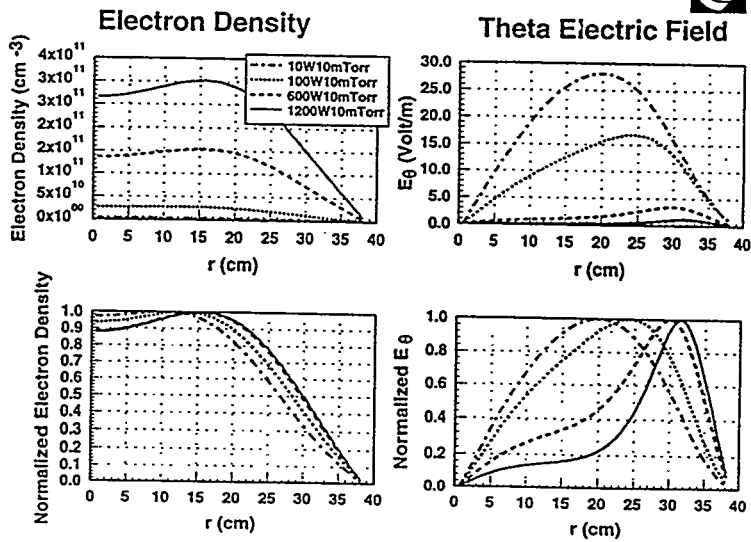
## Basic trends in the Ar simulations

- Plasma density increases with increasing rf power at fixed pressure due to power balance. (density  $\propto$  power, temperature independent of power)
- Plasma density increases with increasing pressure at fixed power due to particle balance. (temperature decreases with pressure leading to a larger density required for power balance)
- At high power, the large electron density leads to small rf skin depths and thus localized heating. At low power, the skin depth is large and more uniform heating results in on axis peaking of the density profile.
- For small skin depths, increasing pressure reduces the electron mean-free-path, decreasing the ability of thermal conductivity to spread the rf power throughout the plasma. This results in enhanced off axis peaking in the ionization rate and the density.

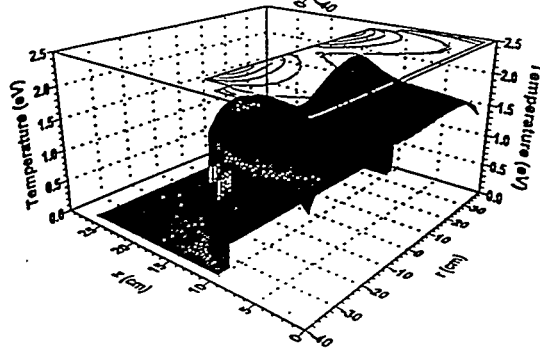
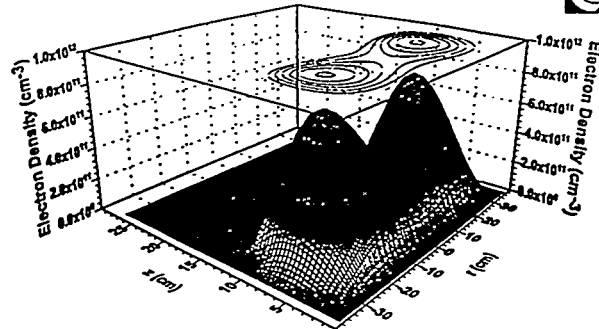
Model radial profiles in Ar as a function of pressure  
1200 w rf power, z ~ 2.125"



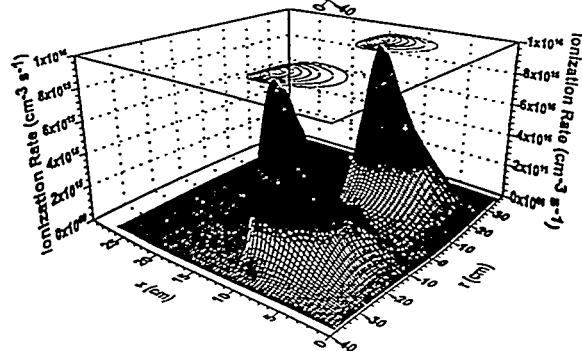
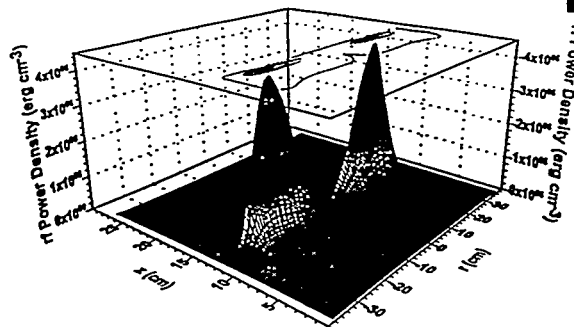
Model radial profiles in Ar as a function of rf power  
10 mTorr, z ~ 2.125"



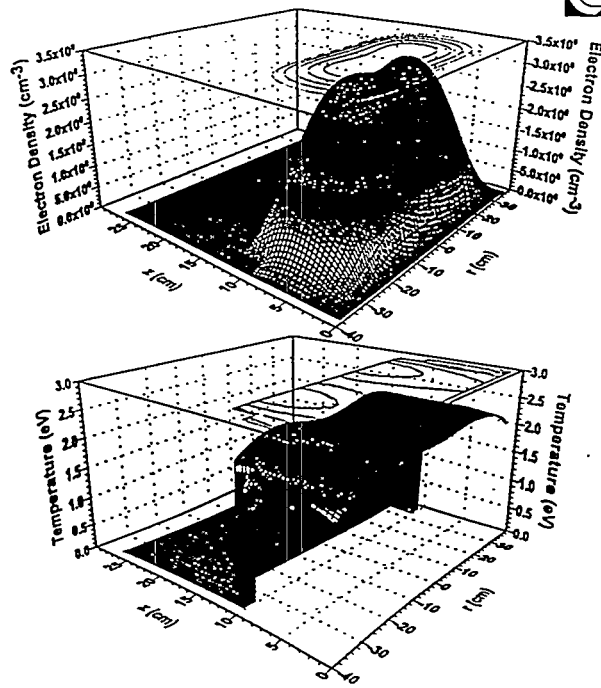
Ar plasma density and temperature in the small skin depth regime (50 mTorr, 1200 w rf power)



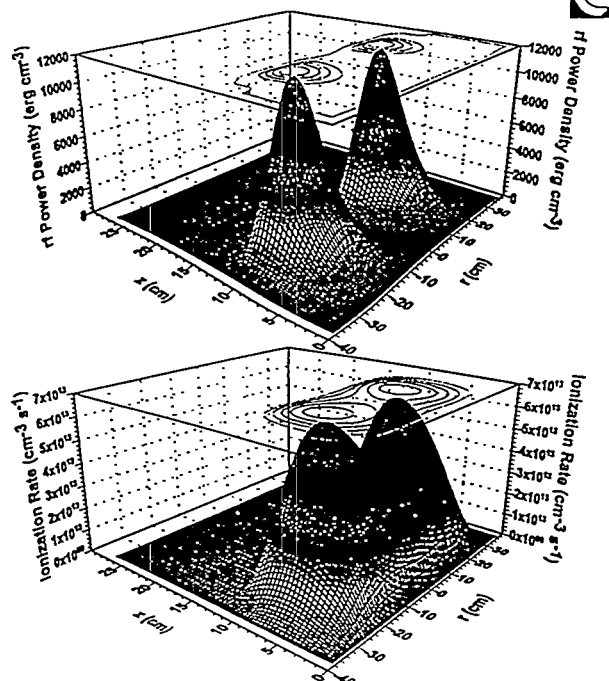
Ar plasma power and ionization in the small skin depth regime (50 mTorr, 1200 w rf power)



Ar plasma density and temperature in the large skin depth regime (10 mTorr, 10 w rf power)



Ar plasma power and ionization in the large skin depth regime (10 mTorr, 10 w rf power)



## Conclusions

---



- We show good uniformity over a 40 cm diameter in the experimental Ar and N<sub>2</sub> data of our large area chamber system.
- The radial profiles of plasma density however show large variations with pressure and rf power.
- Model simulations of Ar duplicate very well the experimental data, allowing us to explore design modifications to regulate the uniformity.